Influence of Cavities on the Structural Performance of Compressed Earth Brick Masonry: A Parametric Comparison of Various Cavity Shapes and Sizes

Simon-Pierre Joy Salassi[1,2(✉)], Philbert Nshimiyimana[1], Decroly Denouwe Djoubissie[1], Adamah Messan[1], and Luc Courard[2]

[1] Laboratoire Eco-Matériaux et Habitats Durables (LEMHaD), Institut International d'Ingénierie de l'Eau et de L'Environnement (Institut 2iE), Ouagadougou, Burkina Faso
joy.salassi@2ie-edu.org, spjsalassi@uliege.be

[2] Urban and Environmental Engineering, Université de Liège, Liège, Belgium

Abstract. The use of masonry, and particularly of geo-sourced materials like compressed earth bricks, has been generating growing interest. These materials represent an alternative to cementitious products such as concrete, thereby reducing the demand for cement. For this substitution to be fully effective, improving their mechanical performance remains a crucial challenge. Although several studies have been conducted on the brick scale, the improvement of the masonry structure may be achieved through the improvement of mortar joints and their interface with the brick. One of the best ways to ensure perfect adhesion of interfaces is to produce full bricks with cavities such that the wet mortar takes the shape of the cavity and anchors itself in the brick as it hardens. Such cavities can influence the global behaviour of masonry. The common shape of the cavity in the CEB is trapezoidal and is located only at the middle top of the brick. This study aims to investigate the real added value of these cavities and to study the influence of the different shapes and sizes of the cavities on masonry behaviour. To achieve this objective, an experimental study and numerical simulations were conducted. In the first approach, a push-out test was performed on triplets formed using bricks without cavities. This first approach allowed to obtain interface parameters such as cohesion and coefficient of friction. The same test was performed numerically using triplets formed by bricks with different cavities. In this second approach, a total of 12 bricks were designed with different shapes and sizes of cavities. The results showed different distributions of stress at the interface with a concentration near the joint protrusions.

Keywords: CEB · Structural masonry · cavity · frog · push-out · shear

1 Introduction

The interface is the weakest element in masonry owing to its lower stiffness compared to that of brick or mortar joints. Multiple studies have characterized the brick-joint interface, with the mixed-mode behaviour of interfaces well-documented in the literature

S. Saloustros and K. Beyer (Eds.): SAHC 2025, RILEM Bookseries 68, pp. 1409–1423, 2026.
https://doi.org/10.1007/978-3-032-16767-5_110

[1–4]. According to Hilsdorf's theory [5], uniaxial compression loading on masonry induces shear stresses at the brick-mortar interface because of the disparate deformation properties of the bricks and mortar. These shear stresses are often responsible for masonry failure, implying that walls with identical units and mortars but different bond treatments exhibit divergent responses under the same load. Rather than relying on adhesives or external reinforcements to improve brick-joint bonds, an innovative brick-shaped design can enhance the shear strength of the assembly.

Previous studies have explored this concept through various approaches. Sandoval et al. [6] experimentally and numerically investigated the influence of mortar spikes penetrating multi-perforated fired earth bricks on the shear response of the interface, employing a detailed micro-modelling strategy. They concluded that mortar spikes significantly affect the shear behaviour depending on the level of compressive normal stress. Gabor et al. [7] analyzed hollow brick masonry through diagonal compression tests, noting that the maximum shear stress at the interfaces coincides with the fracture of either mortar cores or brick webs (i.e., pure shear loading of joint cubic prisms or short beams, where shear behaviour dominates). Ural [8] conducted an extensive experimental campaign on 54 masonry specimens with vertical dowels connected to tuff stone units. Pushout tests on triplets assessed shear performance, and finite element simulations (using LUCAS software) revealed that shear capacity peaks at a dowel diameter of 14 mm and diminishes for larger diameters. Mousavian and Casapulla [9] developed a computational framework for designing interlocking block assemblages, introducing a concave contact model in which the sliding resistance depends on both lock geometry and Coulomb friction. Subsequent work by Casapulla et al. [10] proposed a digital tool to optimize masonry arch cross sections using interlocking blocks with face connectors, highlighting their superior sliding resistance over conventional blocks.

While these studies differ in focus (e.g., mortarless interlocking blocks vs. mortared masonry), they share a unifying principle: enhancing shear capacity through the geometric optimization of brick shapes.

In Burkina Faso, a traditional technique employs compressed earth blocks (CEBs) with cavities (Fig. 1), which are filled with fresh mortar to act as anchors upon hardening, thereby improving the shear resistance. To the best of our knowledge, no study has quantified the contribution of these cavities to the shear behaviour of masonry. To address this gap, the present study investigates the influence of cavity shape on the response of brick-joint triplets via 2D detailed micro-modelling.

2 Materials and Methodology

2.1 Raw Materials

Compressed earth blocks (CEBs) were fabricated using earthen material sourced from Kamboinsin (12°29′02.4″N, 1°33′00.7"W, 317 m altitude), a locality near Ouagadougou, the capital of Burkina Faso. This clayey-rich material extensively characterized in prior studies [11–19], exhibits favourable geotechnical and mineralogical properties.

Fig. 1. Some examples of cavity-bricks found in Burkina Faso

This material was stabilized using agro-industrial by-products: Carbide Calcium Residue noted in the present work CCR (industrial), and Rice Husk Ash noted RHA (agricultural), which was used to partially substitute CCR. The physicochemical properties of these stabilizers are described in detail in [12].

2.2 Bricks and Mortar Manufacturing

Bricks and mortar were produced for material characterization and to determine the input parameters required for the models. The clayey material was dry mixed with 16% CCR and 4% RHA. Subsequently, the optimum moisture content (22.5 wt%), as determined through a standard Proctor test [20], was added and thoroughly mixed to achieve homogeneity. The mixture was then statically compacted into prismatic molds (295 × 140 × 95 mm), as recommended by XP P13–901 [21], using a TESTARAM machine (Appro-Techno, Couvain, Belgium), which applied a pressure of 35 bar [18, 22]. This equipment was validated in previous studies [13, 15, 16, 22, 23].

The joint mortar consisted of a cement: sand: soil blend with proportions of 1: 2.77: 1.38, reflecting common practices in Burkina-Faso. The water content was adjusted to achieve a flow diameter of 145 mm, as reported in [24]. Two mortar geometries were cast: cubic specimens (100 × 100 × 100 mm) for compression testing and prismatic specimens (40 × 40 × 160 mm) for direct tensile testing.

The CEBs and mortars were cured for 45 and 28 days in sealed plastic bags to maintain hydration conditions until curing, drying, and testing.

2.3 Experimental Characterisation

Four key experimental tests were conducted to characterize the materials and obtain the input parameters for numerical modelling: (i) compression tests on bricks and joint mortar, (ii) direct tension tests on bricks, mortar, and their interface, and (iv) push-out tests on brick triplets.

o **Compression test**

Compression tests were conducted on brick specimens (145 × 145 × 95 mm) obtained by bisecting standard molded blocks, and on mortar joint specimens (100 × 100 × 100 mm). The experimental setup featured vertical loading applied to the upper face; two 5 mm-range vertical displacement sensors mounted vertically via quadrant fixtures, and two horizontal displacement sensors to measure transverse deformation (for Poisson's ratio calculation). This identical configuration was maintained for both

a) b) c) d)

Fig. 2. Experimental setup: a) compression test, b) direct traction test, c) direct interface traction, and d) pushout test on brick joint triplets.

brick and mortar specimens Fig. 2-a, ensuring a consistent measurement methodology across the material types.

o **Traction test**

Both brick and mortar specimens were subjected to direct tension testing to characterize their tensile properties. These parameters are essential for accurate material modelling. The samples were bonded to steel mounting bars using Sikadur®-31 + DW high-strength epoxy adhesive [25] (Fig. 2-b). After 24 h of adhesive curing under controlled conditions, the prepared assemblies were mounted on a 3R mechanical testing machine (capacity: 300 kN). Displacement-controlled loading was applied through the upper crosshead. A constant strain rate was maintained at 0.5 mm/min.

The same principle was used to apply a tensile load to the brick-mortar interface. The specimen for this test was manufactured by bonding two 65 × 65 × 4.5 mm bricks with a 15 mm thick mortar joint.

o **Pushout test**

The triplets were assembled in accordance with the RILEM recommendations [26] using the previously described bricks and mortar. Prior to shear strength testing of the brick-joint interface, three different confinement levels (0.1 MPa, 0.3 MPa, and 0.5 MPa) were applied to the specimens, following the requirements specified in [26]. The experimental setup shown in Fig. 2-d was employed for these tests.

This testing procedure allowed the determination of three key interface parameters: cohesion (c), friction angle (μ), and shear stiffness (k_s).

3 Modelling and Simulation Methodology

Following the experimental characterization of the raw materials, brick units, joint mortars, and their interfaces, the obtained parameters were implemented using the commercial finite element analysis software DIANA FEA [27]. A two-dimensional modeling approach was adopted to simulate the mechanical behavior of bricks with various geometric configurations (Fig. 3).

CEBs and mortars were modeled using the Maekawa-Fukuura Concrete Model [27–29]. This model has the advantage of combining both the elastoplastic damage model and total strain crack model.

Several authors have used the elasto-plastic damage model to model masonry units, especially unfired raw earth-brick material [30–32]. Both components (CEB and joint mortar) were discretized using 8-node quadrilateral isoparametric plane stress elements codified as CQ16M in DIANA FEA [27] with a mesh size of 5 mm, which provided satisfactory solution accuracy.

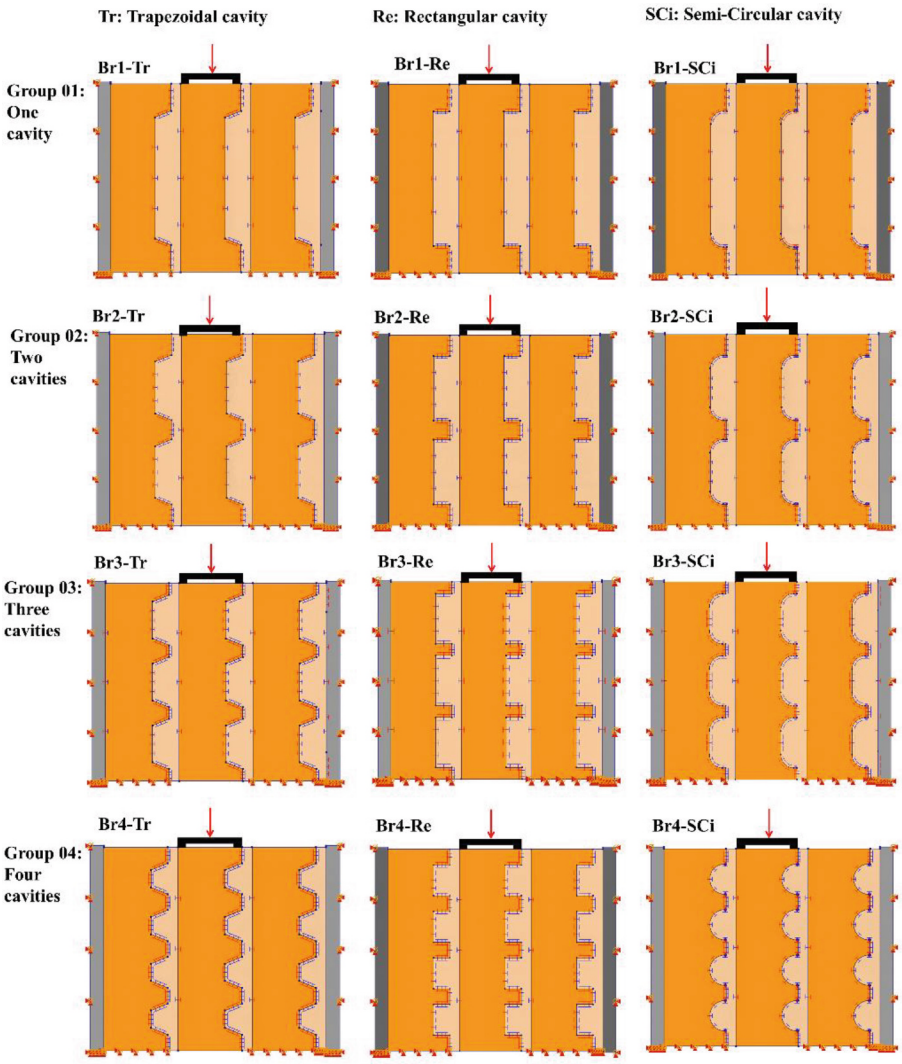

Fig. 3. Presentation of different brick configurations with all boundary conditions.

The brick-mortar interfaces were represented using a combined cracking–shear–crushing (CCSC) model. Initially developed by Lourenço and Rots [33, 34] to capture the entire degradation of brick-joint interfaces subjected to monotonic loads, this model

was improved and extended to cyclic loads by Oliveira et al. [35] and recently by Xie et al. [36]. This model has been used in several studies, such as [37, 38] and recently by Seini-Moussa [39].

In line with the approach adopted by several researchers [7, 39–41], the dilatancy angle was set to zero. This simplification provided conservative results while maintaining analytical tractability, thereby ensuring a safety-oriented approach in the analysis. The specific values of these parameters are listed in Table 1.

A comprehensive parametric study was conducted by simulating pushout tests on 12 distinct brick geometries, systematically categorized into four groups based on cavity configuration: (i) group 1: single cavity (Br1); (ii) group 2: two cavities (Br2); (iii) group 3: three cavities (Br3); and (iv) group 4: four cavities (Br4). Each group included three cavity cross-sectional shapes: trapezoidal (Tr), rectangular (Re), and semicircular (SCi). This classification is illustrated in Fig. 3. All the cavities were maintained at a constant depth of 25 mm throughout the study. To prevent excessive stress on the third bricks caused by the contact of the steel plate with the brick cores, these bricks were filled with joint mortar, which was then in direct contact with the steel plate (Fig. 3). The degrees of freedom of both the steel plates and two extreme CEBs were blocked in both directions, and only the middle brick was left free in the y-direction.

The loading protocol consisted of a single linear load of 30 000 N/m applied to the top of the middle CEB. This load was discretized into 1000 identical incremental load steps to properly capture the nonlinear interface behaviour. Nonlinear resolution was performed using a modified Newton-Raphson method, where the tangent stiffness matrix was updated only at the beginning of each load step to optimize the computational efficiency. Convergence was assessed using an energy-based criterion with a strict tolerance of 0.01%. In cases of non-convergence, an automatic continuation process was activated to subdivide the load step further, ensuring numerical stability and solution accuracy.

The numerical analysis utilized two principal damage evaluation metrics available in the DIANA FEA software [27]: Crack Index (I_{cr}) and maximal shear stress (τ_{max}). The first parameter was calculated according to Eq. (1) [42]. The Crack Index serves as a quantitative indicator of cracking potential within a material. It is mathematically defined as the ratio of the tensile strength f_t of the material to the maximum principal stress σ_I. The maximal shear stress was calculated using Eq. (2).

$$I_{cr} = \frac{f_t}{\sigma_I} \tag{1}$$

$$\tau_{\max} = \frac{\sigma_I - \sigma_{II}}{2} \tag{2}$$

I_{cr}: is the crack index [-];
f_t: the tensile strength of the material [MPa];
σ_I: the principal stress of the material in the first direction [MPa];
σ_{II}: the principal stress of the material in the second direction [MPa];
τ_{max}: the maximal shear stress [MPa].

Within DIANA software implementation, specific threshold values govern the interpretation of I_{cr}. When the maximum principal stress remains extremely low compared with the material tensile strength ($\sigma_I \leq 0.01 f_t$), the software automatically assigns a value of $I_{cr} = 100$, indicating an uncracked, structurally sound section. Conversely, $I_{cr} \leq 1$ signifies the initiation of cracking and structural deterioration.

Table 1. Input parameters for Maekawa-Fukuura model and for CCSC model

Maekawa-Fukuura				CCSC model			
Materials		Brick	Mortar	Brick-Mortar Interface			
Mass density	kg/m^3	2500	1800	Normal stiffness	kN/m^3		1914
Strain at compressive strength	%	0.09	0.04	Shear stiffness	kN/m^3		2980
Tensile strength	MPa	0.3	0.62	Tensile strength	kPa		250
UCS	MPa	8.3	9.5	Fracture energy	kN/m		0.625
Threshold angle between cracks	o	30	0.25	Cohesion	kPa		320
				Friction angle	o		16.65
				Dilatancy angle	o		0
				Res Fric. Angle	o		–
				Mode II fracture energy	a	m	780
					b	kN/m	9.7x10^5
				Compressive strength	kPa		9500
				Factor	Cs		0.2
				Compressive fracture energy	kN/m		1
				Equivalent plastic relative displacement	m		0.002

The analysis was conducted at identical reference points, that is, one node on the central brick (Fig. 6). The present study employs crack index progression analysis by plotting Icr against the load step to (i) precisely identify damage initiation points and (ii) quantitatively evaluate how cavity geometry influences crack resistance. The results demonstrate that the strategic cavity design can effectively delay both crack initiation and subsequent propagation, thereby enhancing structural performance.

The maximum shear stress was plotted against the maximum shear strain. This parameter was used to evaluate the influence of each cavity on the interfacial shear stiffness, defined as the slope of the initial linear portion of the shear stress-strain curve.

4 Results and Discussions

As detailed in Sect. 3, the crack index I_{cr} was analyzed as a function of the load factor λ at the node selected in Fig. 6 to evaluate the damage progression.

Figure 6 further illustrates the ability of each brick to retard the damage. Notably, the bricks with the smallest cavities (represented by yellow curves) exhibited the highest resistance to crack propagation. If the influence of the number and the size of the cavities can be clearly be identified on Fig. 6, the influence of their shape is not clearly identifiable.

Figure 4 illustrates the distribution of the maximal shear stress across each section of the brick setup. The color-scaled results for each brick group indicate consistent crack initiation at the brick and joint corners and webs. The analysis demonstrates that brick webs are the first to undergo damage before they propagate throughout the entire brick. This suggests that bricks with many cavities are more susceptible to cracks than bricks with only one cavity.

Figure 5-a presents the shear stress-strain curves for each triplet setup. Notably, the bricks in Group 2, particularly Br2-Tr and Br-2- Sci exhibit the highest shear stresses, respectively 0.67 MPa and 0.47 MPa. Complementary to Fig. 5-a, Fig. 5-b shows the displacement of the mid-brick against the load factor. The slope of each curve's linear regression is highlighted. This allows to clearly observe the influence of the cavity geometry on the stiffness and displacement. A steeper slope indicated a larger displacement for a given load, indicating that the assembly was less rigid. Figure 5-b shows that the Br2-SCi model (brick with two semi-circular frogs) stands out. It has the shallowest slope, indicating the smallest displacement and, therefore, the highest rigidity. This result demonstrates that the two semi-circular frogs provide the best resistance to sliding at the brick-mortar interface, significantly improving the overall mechanical interlock.

From Fig. 5-a, the slopes of the linear ascending parts of these curves were determined. These slopes were related to the shear stiffness of the interfaces. Figure 7 depicts the influence of each setup on this parameter. The semi-circular shape enhanced the shear stiffness of the interface in the cases of two, three, and four small cavities. Maximal shear stiffness was observed with the Br2-Sci setup. Liu et al. [43] identified the circular shape as the most resilient in mortarless bricks because it enhanced in-plane energy dissipation and improved out-of-plane stability.

The analysis of the Fig. 5 and Fig. 7 allows for a comparison of the shear resistance of the different brick models tested. This analysis reveals that the Br2-Sci model exhibits a significantly superior mechanical behaviour, characterized by the highest interface stiffness and the lowest displacement of the middle brick among all specimens. This

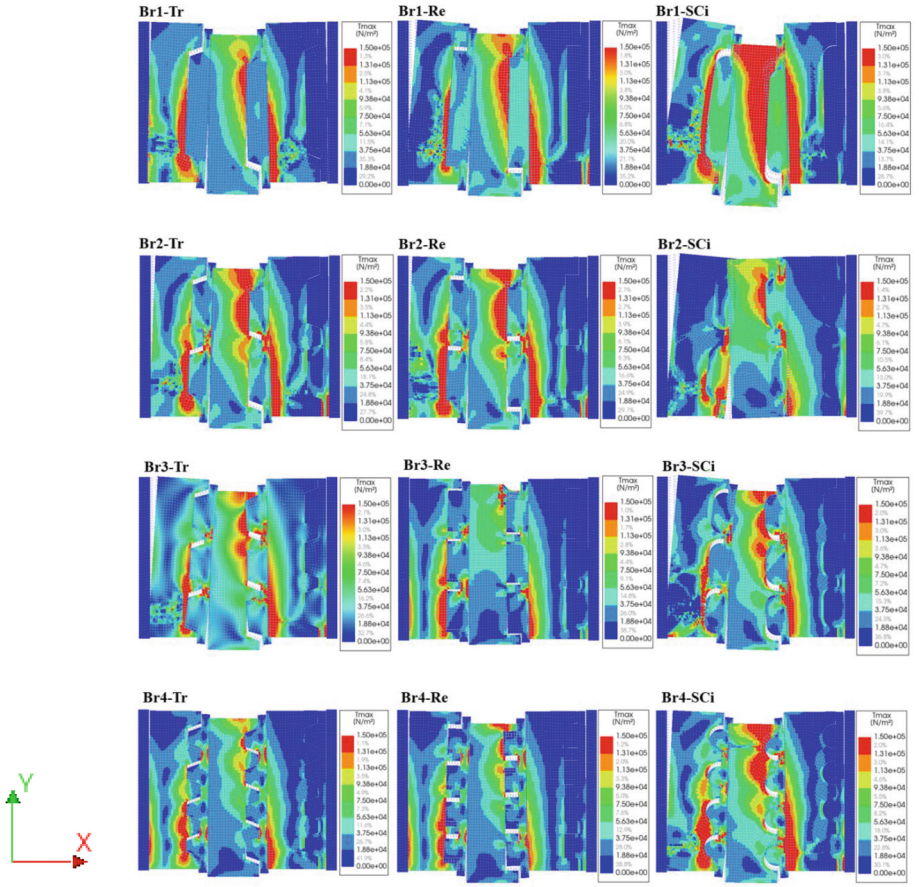

Fig. 4. Maximum shear stress color map

optimization of mechanical properties stems from the efficiency of its anchoring, and the presence of two cavities provides an optimal compromise, offering an increased contact surface with the mortar and generating an effective mechanical interlock phenomenon without overly weakening the brick's structure. Conversely, although they theoretically offer a greater adhesion surface, models with three or four cavities display an increased susceptibility to cracking. Indeed, the multiplication of cavities creates numerous protrusions with sharp edges, which act as stress concentrators and constitute points of fragility where the initiation and propagation of cracks are favoured, leading to premature failure.

Consequently, by avoiding this pitfall, the Br2-Sci geometry is the most promising and robust solution for simultaneously improving the resistance, stiffness, and ductility of masonry structures subjected to shear stress.

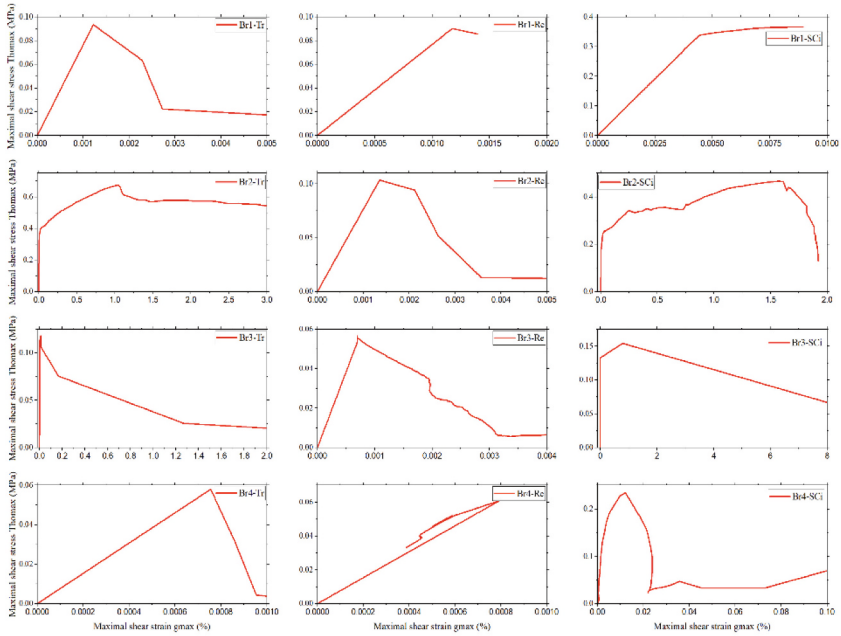

a)

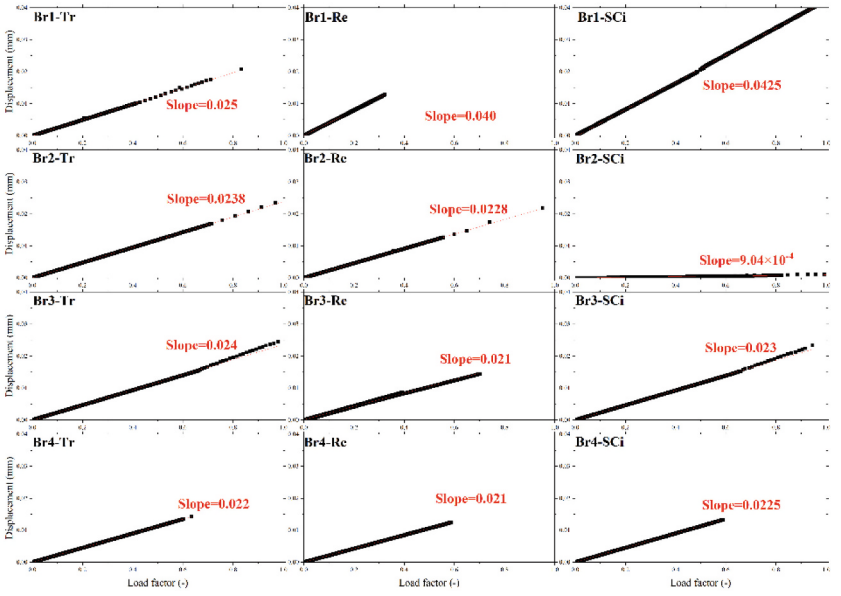

b)

Fig. 5. a) Shear stress versus shear strain curves; b) Mid-brick displacement versus load factor.

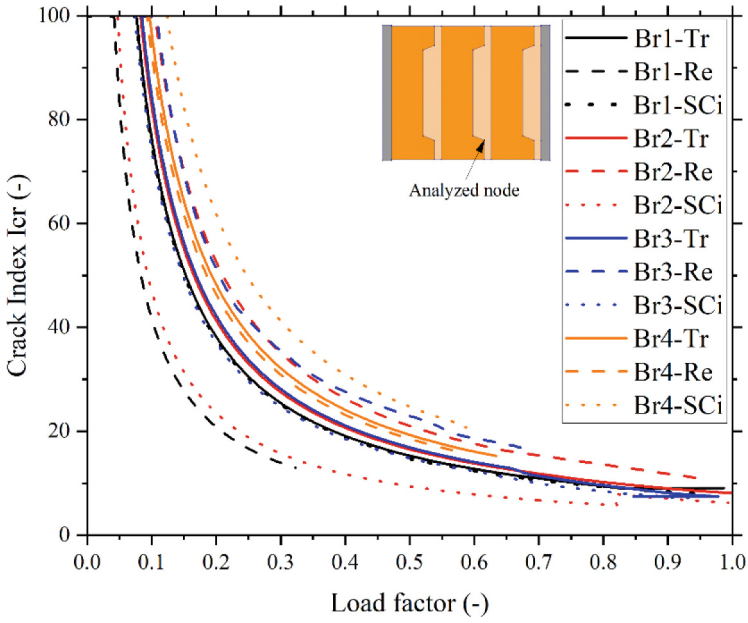

Fig. 6. Crack Index versus load factor at the cavity base

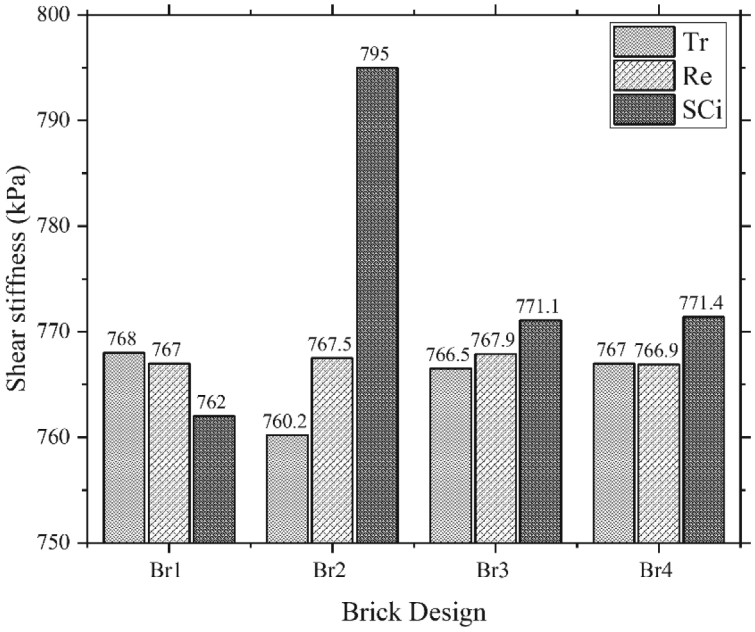

Fig. 7. Shear stiffness of each triplet setup

5 Conclusion

The objective of the present study was to quantitatively assess, through detailed micro-modelling, the contribution of cavities to the shear response of the brick-joint interface. To this end, four distinct groups of bricks were modelled, each featuring different cavity shapes and sizes.

The results showed that bricks with multiple cavities can exhibit high crack susceptibility because of the high stress concentration in the brick and joint protuberance webs. However, bricks with two cavities, one with a trapezoidal shape and the other with a semi-circular shape, exhibited the highest shear strength and stiffness, respectively. This configuration (two cavities) can then be presented as the optimal shape to enhance the shear behavior of the brick-mortar interface.

This work represents the first part of a more comprehensive and extensive study that includes 3D modelling and experimental tests.

References

1. Sauve, M.B.: Etude des ouvrages maçonnés en pierre par la méthode des éléments discretes: caractérisation et modélisation du comportement cohésif des joints. PhD, Ecole doctorale des sciences physiques et de l'Ingénierie, Université de Bordeaux (2016)
2. Dimitri, R., Trullo, M., De Lorenzis, L., Zavarise, G.: Coupled cohesive zone models for mixed-mode fracture: a comparative study. Eng. Fract. Mech. **148**, 145–179 (2015). https://doi.org/10.1016/j.engfracmech.2015.09.029
3. Hamid Lofti, B.S., Members ASCE. Interfade model applied to fracture of masonry structures. J. Struct. Eng. **120**, 63–80 (1944)
4. Sacco, E., Lebon, F.: A damage–friction interface model derived from micromechanical approach. Int. J. Solids Struct. **49**(26), 3666–3680 (2012). https://doi.org/10.1016/j.ijsolstr.2012.07.028
5. Hilsdorf, H.K.: Investigation into failure mechanism of brick masonry loaded in axial compression. In: The International Conference on Masonry Structures Systems, University of Texas, D. F. Johnson, Ed., 1969: Gulf Publishing Company
6. Sandoval, C., Arnau, O.: Experimental characterization and detailed micro-modeling of multi-perforated clay brick masonry structural response. Mater. Struct. **50**(1) (2016). https://doi.org/10.1617/s11527-016-0888-3
7. Gabor, A., Ferrier, E., Jacquelin, E., Hamelin, P.: Analysis and modelling of the in-plane shear behaviour of hollow brick masonry panels. Constr. Build. Mater. **20**(5), 308–321 (2006). https://doi.org/10.1016/j.conbuildmat.2005.01.032
8. Ural, A.: Triplet tests and numerical validations of stone masonry with dowels under shear. Arab. J. Sci. Eng. **46**, 14 (2021). https://doi.org/10.1007/s13369-020-05152-8
9. Casapulla, E.M.C., Zarghani, M.: A digital tool to design structurally feasible semi-circular masonry arches composed of interlocking blocks. Comput. Struct. **221**, 15 (2019)

10. Casapulla, E.M.C.: Structurally informed design of interlocking block assemblages using limit analysis. J. Comput. Design Eng. **7**(4), 20 (2020). https://doi.org/10.1093/jcde/qwaa038
11. Nshimiyimana, P., Miraucourt, D., Messan, A., Courard, L.: Calcium carbide residue and rice husk ash for improving the compressive strength of compressed earth blocks. MRS Adv. **3**(34–35), 2009–2014 (2018). https://doi.org/10.1557/adv.2018.147
12. Nshimiyimana, P.: Effect of the type of clay earthen materials and substitution materials on the physico-mechanical properties and durability of compressed earth blocks., PhD, Laboratoire Eco-Matériaux et Habitats Durables (LEMHaD), Institute 2iE GeMMe - Building Materials, Urban and Environmental Engineering (UEE), ULiege, Institut 2iE, Université de Liège (2020)
13. Djibo, K.B., Sore, S.O., Nshimiyimana, P., Akodenyon, D.Y., Messan, A.: Hydromechanical performances and durability of compressed earth blocks stabilised with metakaolin-based geopolymer binder. Mater. Struct. **57**(7) (2024). https://doi.org/10.1617/s11527-024-02446-3
14. P. Nshimiyimana, P., Messan, A., Zhao, Z., Courard, L.: Chemico-microstructural changes in earthen building materials containing calcium carbide residue and rice husk ash. Constr. Build. Mater. **216**, 622–631 (2019). https://doi.org/10.1016/j.conbuildmat.2019.05.037
15. Philbert, N., Césaire, H., Omar, S.S., Ousmane, Z., Adamah, M., Luc, C.: Durability performances of compressed earth blocks exposed to wetting-drying cycles and high temperature. Eco-Architecture IX **210**, 141–149 (2022). https://doi.org/10.2495/ARC220121
16. Nshimiyimana, P., Messan, A., Courard, L.: Hydric and durability performances of compressed earth blocks stabilized with industrial and agro by-product binders: calcium carbide residue and rice husk ash. J. Mater. Civil Eng. **33**(6) (2021). https://doi.org/10.1061/(asce)mt.1943-5533.0003745
17. Nshimiyimana, P., Fagel, N., Messan, A., Wetshondo, D.O., Courard, L.: Physico-chemical and mineralogical characterization of clay materials suitable for production of stabilized compressed earth blocks. Constr. Build. Mater. **241** (2020). https://doi.org/10.1016/j.conbuildmat.2020.118097
18. Nshimiyimana, P., Messan, A., Courard, L.: Physico-mechanical and hygro-thermal properties of compressed earth blocks stabilized with industrial and agro by-product binders. Materials (Basel) **13**(17) (2020). https://doi.org/10.3390/ma13173769
19. Nshimiyimana, P., Hema, C., Zoungrana, O., Messan, A., Courard, L.: Thermophysical and mechanical properties of compressed earth blocks containing fibres: by-product of Okra plant and polymer waste. Eco-Architecturee VIII **195**, 149–161 (2020). https://doi.org/10.2495/ARC200121
20. NF P 94–093. Détermination des références de compactage d'un matériau, A. F. d. Normalisation, Tour Europe 92049 Paris La Défense Cedex (1999)
21. XP P13–901- 2017 Blocs de terre comprimée pour murs et cloisons, A. F. d. Normalisation, 11, Avenue Francis de Pressensé-93571 Saint-Denis La Plaine Cedex (2017)
22. Omar Sore, S., Messan, A., Prud'homme, E., Escadeillas, G., Tsobnang, F.: Stabilization of compressed earth blocks (CEBs) by geopolymer binder based on local materials from Burkina Faso. Constr. Build. Mater. **165**, 333–345 (2018). https://doi.org/10.1016/j.conbuildmat.2018.01.051
23. Dime, T., Sore, S.O., Nshimiyimana, P., Messan, A., Courard, L.: Comparative study of the reactivity of clay earth materials for the production of compressed earth blocks in ambient conditions: effect on their physico-mechanical performances. J. Miner. Mater. Charact. Eng. **10**(01), 43–56 (2022). https://doi.org/10.4236/jmmce.2022.101004
24. Testing fresh concrete, B. S. Publication, 31 august 2010 (2010)

25. S. F. S.A.S. Notice Produit. ed. 84 rue Edouard Vaillant, 93350 LE BOURGET, FRANCE: Sika France (2023)
26. RILEM TC 127-MS: Tests for masonry materials and structures, R. T. Commitees, Building Research Establishment, Watford, WD2 7JR, UK (1996)
27. D. F. E. Analysis, DIANA Documentation Release 10.5. Thijsseweg 11, 2629 JA Delft, The Netherlands: DIANA FEA Bv (2022)
28. Koichi Maekawa, J.-i.T., Irawan, P., Irie, M: Continuum fracture in concrete nonlinearity under triaxial confinement. Presented in Proceedings of JSCE 02/1993, 460 (1993)
29. Koichi Maekawa, J.-i.T., Irawan, P., Irie, M.: Plasticity in concrete nonlinearity under triaxial confinement. Presented in Proceedings of JSCE 02/1993, 460 (1993)
30. Kumar, N., Barbato, M., Rengifo-López, E.L., Matta, F.: Finite element detailed micromodeling of unreinforced earth block masonry. J. Struct. Eng. **149**(7) (2023). https://doi.org/10.1061/jsendh.Steng-12093
31. Rainone, L.S., Tateo, V., Casolo, S., Uva, G.: About the use of concrete damage plasticity for modeling masonry post-elastic behavior. Buildings **13**(8) (2023). https://doi.org/10.3390/buildings13081915
32. AlGohi, B.H., Baluch, M.H., Rahman, M.K., Al-Gadhib, A.H., Demir, C.: Plastic-damage modeling of unreinforced masonry walls (URM) subject to lateral loading. Arab. J. Sci. Eng. **42**(9), 4201–4220 (2017). https://doi.org/10.1007/s13369-017-2626-8
33. Lourenço, P.B.: Computational Strategies for Masonry Structures. Faculdade de Engenharia a Universidade do Porto, Portugal (1996)
34. Paulo Lourenço, J.R.: Multisurface interface model for analysis of masonry structures. J. Eng. Mech. **123**, 8 (1997)
35. Oliveira, D.V., Lourenço, P.B.: Implementation and validation of a constitutive model for the cyclic behaviour of interface elements. Comput. Struct. **82**(17–19), 1451–1461 (2004). https://doi.org/10.1016/j.compstruc.2004.03.041
36. Xie, Z., Sousamli, M., Messali, F., Rots, J.G.: A sub-stepping iterative constitutive model for cyclic cracking-crushing-shearing in masonry interface elements. Comput. Struct. **257** (2021). https://doi.org/10.1016/j.compstruc.2021.106654
37. van Zijl, G.P.A.G.: Modeling masonry shear-compression: role of dilatancy highlighted. J. Eng. Mech. **130**(11), 1289–1296 (2004). https://doi.org/10.1061/(asce)0733-9399(2004)130:11(1289)
38. Francesca da Porto, G.G., Garbin, E., Modena, C.: In-plane behavior of clay masonry walls: experimental testing and finite-element modeling. J. Struct. Eng. **136**(11), 1379–1392 (2010). https://doi.org/10.1061/(ASCE)ST.1943-541X.0000236
39. Moussa, H.S.: Etude du comportement hydromécanique des maçonneries en blocs de latérite taillée (BLT) au Burkina Faso. PhD, Ecole doctorale Sciences et Technologies de l'eau, de l'énergie et de l'environnement, Institut 2iE, Ouagadougou, Burkina Faso (2025)
40. Sarhosis, V., Garrity, S.W., Sheng, Y.: Influence of brick–mortar interface on the mechanical behaviour of low bond strength masonry brickwork lintels. Eng. Struct. **88**, 1–11 (2015). https://doi.org/10.1016/j.engstruct.2014.12.014
41. Gajjar, E.G.P.N., Martin-Alarcon, D.C., Pereira, J., Lourenço, P., Colla, C.: An experimental and numerical contribution for understanding the in-situ shear behaviour of unreinforced masonry. J. Build. Eng. **44** (2021). https://doi.org/10.1016/j.jobe.2021.103389

42. standard specificatipons for concrete structures, J. S. o. C. E. JSCE (2024)
43. Liu, H., Liu, P., Lin, K., Zhao, S.: Cyclic behavior of mortarless brick joints with different interlocking shapes. Materials (Basel) **9**(3) (2016). https://doi.org/10.3390/ma9030166